Kinetics of α-Hydroxy-alkylperoxyl Radicals in Oxidation Processes. $HO_2^{\bullet}$-Initiated Oxidation of Ketones/Aldehydes near the Tropopause

Ive Hermans,[†,‡] Jean-François Müller,[§] Thanh Lam Nguyen,[†] Pierre A. Jacobs,[‡] and Jozef Peeters*[,†]

Division of Quantum Chemistry and Physical Chemistry, Department of Chemistry, KULeuven, Celestijnenlaan 200F, B-3001 Heverlee, Belgium, Centre for Surface Chemistry and Catalysis, Department of Interphase Chemistry, KULeuven, Kasteelpark Arenberg 23, B-3001 Heverlee, Belgium, and Belgian Institute for Space Aeronomy, Avenue Circulaire 3, B-1180 Brussels, Belgium

Received: December 29, 2004; In Final Form: March 7, 2005

A comparative theoretical study is presented on the formation and decomposition of α-hydroxy-alkylperoxyl radicals, Q(OH)OO$^{\bullet}$ (Q = RR′C:), important intermediates in the oxidation of several classes of oxygenated organic compounds in atmospheric chemistry, combustion, and liquid-phase autoxidation of hydrocarbons. Detailed potential energy surfaces (PESs) were computed for the $HOCH_2O_2^{\bullet} \rightleftharpoons HO_2^{\bullet} + CH_2O$ reaction and its analogues for the alkyl-substituted RCH(OH)OO$^{\bullet}$ and $R_2C(OH)OO^{\bullet}$ and the cyclic *cyclo*-$C_6H_{10}(OH)OO^{\bullet}$. The state-of-the-art ab initio methods G3 and CBS-QB3 and a nearly converged G2M//B3LYP-DFT variant were found to give quasi-identical results. On the basis of the G2M//B3LYP-DFT PES, the kinetics of the ≈15 kcal/mol endothermal α-hydroxy-alkylperoxyl decompositions and of the reverse $HO_2^{\bullet}$ + ketone/aldehyde reactions were evaluated using multiconformer transition state theory. The excellent agreement with the available experimental (kinetic) data validates our methodologies. Contrary to current views, $HO_2^{\bullet}$ is found to react as fast with ketones as with aldehydes. The high forward and reverse rates are shown to lead to a fast Q(OH)OO$^{\bullet} \rightleftharpoons HO_2^{\bullet}$ + carbonyl quasi-equilibrium. The sizable [Q(OH)OO$^{\bullet}$]/[carbonyl] ratios predicted for formaldehyde, acetone, and *cyclo*-hexanone at the low temperatures (below 220 K) of the earth's tropopause are shown to result in efficient removal of these carbonyls through fast subsequent Q(OH)OO$^{\bullet}$ reactions with NO and $HO_2^{\bullet}$. IMAGES model calculations indicate that at the tropical tropopause the $HO_2^{\bullet}$-initiated oxidation of formaldehyde and acetone may account for 30% of the total removal of these major atmospheric carbonyls, thereby also substantially affecting the hydroxyl and hydroperoxyl radical budgets and contributing to the production of formic and acetic acids in the upper troposphere and lower stratosphere. On the other hand, an RRKM−master equation analysis shows that hot α-hydroxy-alkylperoxyls formed by the addition of O_2 to C_1-, C_2-, and C_3-α-hydroxy-alkyl radicals will quasi-uniquely fragment to $HO_2^{\bullet}$ plus the carbonyl under all atmospheric conditions.

Introduction

Decomposition reactions of $HOR_{-H}OO^{\bullet}$ α-hydroxy-alkylperoxyl radicals (further denoted as Q(OH)OO$^{\bullet}$, with Q = H_2C:, RHC:, or RR′C:) are frequently encountered in both atmospheric chemistry[1,2] and combustion.[3] The Q(OH)OO$^{\bullet}$ radicals are often produced by the fast addition of O_2 to α-hydroxy-alkyl radicals formed by α-hydrogen abstraction from an alcohol by $^{\bullet}$OH or $HO_2^{\bullet}/RO_2^{\bullet}$ radicals. Experimental work by Lesclaux and coworkers[4,5] revealed that α-hydroxy-alkylperoxyl radicals eliminate $HO_2^{\bullet}$ quite fast to form the corresponding carbonyl compound (denoted Q═O):

$$Q(OH)OO^{\bullet} \rightarrow Q{=}O + HOO^{\bullet} \qquad (r.1)$$

Various authors have shown that this reaction proceeds via a cyclic, hydrogen-bonded intermediate complex, *c*-(Q═O···HOO$^{\bullet}$), that can either revert to the reactant or decompose to the end products:[6−8]

$$Q(OH)OO^{\bullet} \rightarrow TS\mathit{a} \rightarrow \mathit{c}\text{-}(Q{=}O\cdots HOO^{\bullet}) \qquad (k_{+}a)$$

$$\mathit{c}\text{-}(Q{=}O\cdots HOO^{\bullet}) \rightarrow TS\mathit{a} \rightarrow Q(OH)OO^{\bullet} \qquad (k_{-}a)$$

$$\mathit{c}\text{-}(Q{=}O\cdots HOO^{\bullet}) \rightarrow TS\mathit{b} \rightarrow Q{=}O + HOO^{\bullet} \qquad (k_{+}b)$$

TS*a* is the five-membered cyclic hydrogen-bonded transition state for the concerted $HO_2^{\bullet}$ elimination/addition, whereas TS*b* is the variational transition state for hydrogen-bond formation/breaking between $HO_2^{\bullet}$ and Q═O.

In this work, a master equation analysis will be performed to investigate the fates of the chemically activated C_1-C_3 and *cyclo*-C_6 Q(OH)OO$^{\bullet}$ radicals arising from Q$^{\bullet}$(OH) + O_2 → Q(OH)OO$^{\bullet}$ with initial energies of about 40 kcal/mol, which can either collisionally stabilize, redissociate to Q$^{\bullet}$(OH) + O_2, or decompose to Q═O + $HO_2^{\bullet}$. We will also examine the reverse addition of $HO_2^{\bullet}$ to carbonyl compounds to form Q(OH)OO$^{\bullet}$, a reaction type that is known to be moderately fast for aldehydes[4,5] but is generally thought to be negligible for ketones.[9]

In liquid-phase hydrocarbon autoxidation literature, it has been assumed thus far that (thermalized) Q(OH)OO$^{\bullet}$ radicals

* Corresponding author. E-mail: jozef.peeters@chem.kuleuven.ac.be.
† Department of Chemistry, KULeuven.
‡ Department of Interphase Chemistry, KULeuven.
§ Belgian Institute for Space Aeronomy.

10.1021/jp044080v CCC: $30.25
Published on Web 04/14/2005

abstract hydrogen atoms from the hydrocarbon substrate to form Q(OH)OOH, or react with other peroxyl radicals.[10] In the present paper, the thermal decomposition, $Q(OH)OO^{\bullet} \rightarrow Q{=}O + HO_2^{\bullet}$, will be shown to be the predominant reaction path—which can significantly influence autoxidation kinetics[11] as $HO_2^{\bullet}$ radicals are known to terminate rapidly with the chain-carrying peroxyl radicals.[12]

The concerted addition of $HO_2^{\bullet}$ to carbonyls to form Q(OH)-$OO^{\bullet}$ will be carefully examined, as preliminary work of ours[13] indicates that these reactions may be of importance at the lowest atmospheric temperatures. The atmospheric implications of such $HO_2^{\bullet}$-initiated oxidation of carbonyl compounds will be further investigated using model calculations.

Although specific $Q(OH)OO^{\bullet}$ radicals are addressed here, that is, Q = CH_2, CH_3CH, $(CH_3)_2C$, and *cyclo*-C_6H_{10} (*cyclo*-hexylidene), general conclusions can be drawn as to the reactivity of (larger) analogous radicals under various conditions.

Computational Section

All calculations were carried out using the GAUSSIAN 03 program.[14] High-level, single-point G2M[15] calculations were performed to evaluate the energies of critical points on the potential energy surfaces (PESs). To verify the influence of the CCSD(T) basis set, various G2M calculations were performed. In this work, G2M*a*//DFT denotes E[UCCSD(T)/6-31G(d)//B3LYP/cc-pVTZ] + {E[UMP2/6-311++G(3df,3pd)//B3LYP/cc-pVTZ]−E[UMP2/6-31G(d)//B3LYP/cc-pVTZ]} + ZPE[B3LYP/cc-pVTZ], G2M*b*//DFT equals E[UCCSD(T)/6-311G(d,p)//B3LYP/cc-pVTZ] + {E[UMP2/6-311++G(3df,3pd)//B3LYP/cc-pVTZ]−E[UMP2/6-311G(d,p)//B3LYP/cc-pVTZ]} + ZPE[B3LYP/cc-pVTZ], and G2M*c*//DFT equals E[UCCSD(T)/aug-cc-pVDZ//B3LYP/cc-pVTZ] + {E[UMP2/aug-cc-pVTZ//B3LYP/cc-pVTZ]−E[UMP2/aug-cc-pVDZ//B3LYP/cc-pVTZ]} + ZPE[B3LYP/cc-pVTZ]. Clearly, G2M*c*//DFT is the method of choice, but it is computationally prohibitive for larger systems as for Q = *cyclo*-hexylidene (*c*-C_6H_{10}). Yet, the systematic (slight) energy differences between the three G2M levels found for smaller systems can be used to address the larger structures at moderate computational cost. The G2M*c*//DFT single-point energies are found to be in excellent agreement with the CBS-QB3[16] and G3[17] results. Frequency analyses and intrinsic reaction coordinate (IRC) calculations identified the located stationary points on the PES as true minima or as saddle-point transition states (TSs) connecting the reactants and products by paths of steepest descent. Spin contamination of the wave functions was found to be negligible for all species involved ($\langle S^2 \rangle$ before spin annihilation ≈0.76 for PES minima and ≈0.77 for TS*a*). Variational transition states were localized by scanning the PES at the B3LYP/6-311++G(d,p) level of theory and identified as the bottleneck structure that minimizes the rate constant. Thermal rate constants of elementary reaction steps were evaluated using multiconformer transition state theory (MC-TST).[18,19] However, the rate constants under conditions where the high-pressure limit is not reached require correction for the falloff factor, which was calculated using the appropriate Rice−Ramsperger−Kassel−Marcus (RRKM) expressions.[20] The vibration partition function of the reactant, the vibration density of states of the reactant, and the number of accessible states of the TS—with the latter two counted directly by the Beyer−Swinehart−Stein−Rabinovitch algorithm with a grain size of 1 cm^{-1}—were calculated taking into account all relevant reactant conformers, using the B3LYP/cc-pVTZ vibration frequencies and energy spacings of the rotamers and the (extrapolated) G2M*c*//DFT barrier height.

TABLE 1: Relative Energies (kcal/mol), ZPE-Corrected, of the Stationary Points on the PES of the $CH_2(OH)OO^{\bullet} \rightleftharpoons H_2C{=}O + HO_2^{\bullet}$ Reaction at Various High Levels of Theory

structure[a]	G3	G2M*a*// DFT[b]	G2M*b*// DFT[b]	G2M*c*// DFT[b]
$^{\bullet}CH_2OH + O_2$	35.9	35.2	35.2	34.8
$CH_2(OH)OO^{\bullet}$_pm	0.0	0.0	0.0	0.0
$CH_2(OH)OO^{\bullet}$_pp	1.4	1.4	1.4	1.4
$CH_2(OH)OO^{\bullet}$_pt	1.5	1.5	1.5	1.5
TS*a*	14.5	14.8	13.6	13.5
c-($H_2C{=}O^{\bullet}\cdot\cdot HOO^{\bullet}$)	8.0	8.0	7.9	8.2
$H_2C{=}O + HOO^{\bullet}$	14.5	15.2	15.3	15.6

[a] The conformers are named according to their HOCO and OOCO dihedral angles. "m" stands for a dihedral angle close to ∼ −60°, "p", close to ∼ +60°, and "t", close to ∼180°. pm and mp, pp and mm, and pt and mt are mirror structures and have equal energy; in the TST rate constant calculations, this is accounted for in the reaction path degeneracy, L^*. [b] The E_{rel} values of the $CH_2(OH)OO^{\bullet}$ conformers with respect to the lowest-lying are calculated at the B3LYP/cc-pVTZ level.

TABLE 2: ZPE-Corrected Energies of the Critical Points on the PES of the $CH_2(OH)OO^{\bullet} \rightleftharpoons H_2C{=}O + HO_2^{\bullet}$ Reaction in kcal/mol—Comparison between Our Work and Literature Data

structure	G2M*c*// DFT[a]	CCSD(T)/cc-pVTZ// CASSCF/6-311G(d,p)[b]	CBS-QB3[c]
$^{\bullet}CH_2OH + O_2$	34.8	32.5	35.8
$CH_2(OH)OO^{\bullet}$	0.0	0.0	0.0
TS*a*	13.5	12.9	13.6
c-($H_2C{=}O^{\bullet}\cdot\cdot HOO^{\bullet}$)	8.2	6.8	8.3
$H_2C{=}O + {}^{\bullet}OOH$	15.6	13.7	15.5

[a] This work. [b] Reference 7. [c] Reference 8.

Under chemical activation conditions, RRKM theory was used to calculate the energy-specific rate constants.[20] Weak-collision master equation analyses were performed to predict the time history of the species involved by an exact stochastic method (ESM).

Results and Discussion

1. Quantum-Chemical Results: Potential Energy Surfaces. Thus far, only the decomposition of $CH_2(OH)OO^{\bullet}$ has been theoretically investigated in some detail.[6−8] Table 1 lists our relative energies of the stationary points on the PES of this reaction at various high levels of theory, whereas Table 2 compares these results with the literature data. Olivella et al.[7] also explored other possible reaction paths such as the internal hydrogen shift $CH_2(OH)OO^{\bullet} \rightarrow CH_2(O^{\bullet})OOH$, the non-hydrogen-bond-assisted $HO_2^{\bullet}$ addition to CH_2O, and the four-center $HO_2^{\bullet}$ addition to formaldehyde, finding the transition states for all of these paths far too high in energy to be of any importance. Therefore, for $CH_2(OH)OO^{\bullet}$ and the other cases, we restricted the analysis to the hydrogen-bond-assisted decomposition, proceeding through the low-lying, fairly tight TS in which the terminal O of $HO_2^{\bullet}$ moves to the carbonyl C, concerted with a hydrogen transfer from $HO_2^{\bullet}$ to the carbonyl O (see Figure 1).

The computational results for the $CH_3CH(OH)OO^{\bullet} \rightleftharpoons CH_3CHO + HO_2^{\bullet}$ reaction are given in Table 3.

Tables 1 and 3 reveal small, systematic differences between the three G2M//DFT levels, also indicating that G2M*c*//DFT is a nearly converged variant of G2M. The energies of the TS structures appear to be more sensitive to the CCSD(T) basis set than the PES minima.

Unfortunately, for systems larger than five heavy atoms, G2M*c*//DFT calculations become computationally too demanding. Yet, using the systematic differences between the various G2M//DFT levels, the lower-level G2M*a*//DFT and G2M*b*//DFT

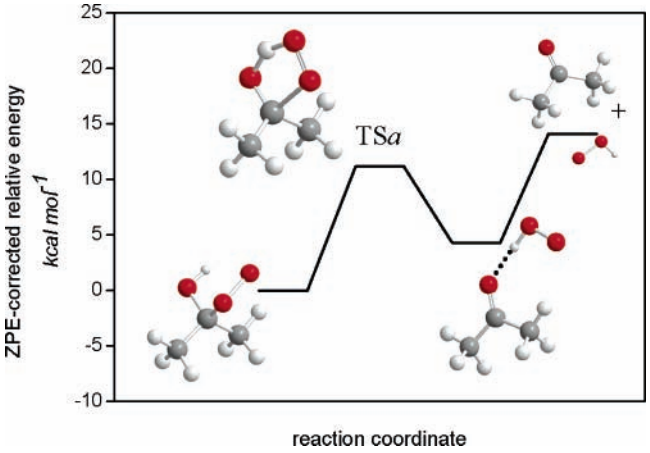

Figure 1. B3LYP-DFT/cc-pVTZ-optimized structures of the stationary points on the PES of the $(CH_3)_2C(OH)OO^\bullet \rightleftharpoons (CH_3)_2C{=}O + HO_2^\bullet$ reaction, including the concerted TS*a* and the hydrogen-bonded complex *c*-$((CH_3)_2C{=}O^\bullet\cdot\cdot HO_2^\bullet)$. The lowest-energy conformers are depicted. Energies, in kilocalories per mole, at the approximated G2M*c*//DFT level (see text).

TABLE 3: Relative Energies (kcal/mol), ZPE-Corrected, of the Stationary Points on the PES of the $CH_3CH(OH)OO^\bullet \rightleftharpoons CH_3CH{=}O + HO_2^\bullet$ Reaction at Various Levels of Theory

structure[a]	G3	CBS-QB3	G2M*a*//DFT[b]	G2M*b*//DFT[b]	G2M*c*//DFT[b]
$CH_3C^\bullet HOH + O_2$	39.4	39.1	38.6	38.7	38.1
$CH_3CH(OH)OO^\bullet$_mp	0.0	0.0	0.0	0.0	0.0
$CH_3CH(OH)OO^\bullet$_pm	1.1	1.1	1.1	1.1	1.1
$CH_3CH(OH)OO^\bullet$_mt	1.6	1.6	1.6	1.6	1.6
$CH_3CH(OH)OO^\bullet$_pt	2.2	2.2	2.2	2.2	2.2
$CH_3CH(OH)OO^\bullet$_mm	2.3	2.3	2.3	2.3	2.3
$CH_3CH(OH)OO^\bullet$_pp	2.6	2.6	2.6	2.6	2.6
TS*a*	13.1	12.8	14.1	12.8	12.5
c-$(CH_3CH{=}O^\bullet\cdot\cdot HOO^\bullet)$	5.9	6.2	5.8	5.7	5.9
$H_3CCH{=}O + HOO^\bullet$	14.7	14.8	14.6	14.8	14.6

[a] The conformers are named as in Table 1. All reactant conformers as well as TS*a* have optical enantiomers of equal energy, which are accounted for in the reaction path degeneracy, L^*. [b] The E_{rel} values of the $CH_3CH(OH)OO^\bullet$ conformers with respect to the lowest-lying are computed at the B3LYP/cc-pVTZ level.

results can be *upgraded* to an approximated G2M*c*//DFT level. The results of the calculations and upgrading extrapolations for Q = $(CH_3)_2C$ and *c*-C_6H_{10} are given in Tables 4 and 5, respectively. A clear inductive trend can be observed: the transition states as well as the decomposition products are increasingly stabilized relative to the $Q(OH)OO^\bullet$ radical as the number and size of the R-substituent(s) on the α-carbon become larger; the Q = *cyclo*-hexylidene case shows in addition a ring-strain effect, destabilizing the TS and the products (see Figure 2).

Internal alkane-hydrogen abstraction by the peroxyl functionality through a six-membered cyclic TS can occur only in the *c*-$C_6H_{10}(OH)OO^\bullet$ radical; as this 1,5-hydrogen shift was found to face a barrier of 30.4 kcal/mol—and the 1,4-hydrogen shift even 37.0 kcal/mol—(B3LYP/6-311++G(d,p) level), such reaction paths cannot compete with the decomposition reaction (r.1).

It must be noted at this point that, in calculating the partition function of acetone, the CH_3-group rotations were treated appropriately as one-dimensional hindered internal rotations, using the approximate quantum solution of Truhlar.[21] Details can be found in the Supporting Information of ref 13.

The quantum-chemical results in Tables 1−4 show that the G2M data are in excellent agreement with both the G3 and CBS-

TABLE 4: Relative Energies (kcal/mol), ZPE-Corrected, of the Stationary Points on the PES of the $(CH_3)_2C(OH)OO^\bullet \rightleftharpoons (CH_3)_2C{=}O + HO_2^\bullet$ Reaction at Different Levels of Theory

structure[a]	G3	CBS-QB3	G2M*a*//DFT[b,c]	G2M*b*//DFT[b,c]	upgraded to approximate G2M*c*//DFT[b,c]
$(CH_3)_2C^\bullet OH + O_2$	40.6	40.0	39.7	39.9	39.3
$(CH_3)_2C(OH)OO^\bullet$_pm	0.0	0.0	0.0	0.0	0.0
$(CH_3)_2C(OH)OO^\bullet$_pt	1.7	1.7	1.7	1.7	1.7
$(CH_3)_2C(OH)OO^\bullet$_pp	2.2	2.2	2.2	2.2	2.2
TS*a*	11.4	11.5	12.6	11.3	11.15
c-$((CH_3)_2C{=}O^\bullet\cdot\cdot HOO^\bullet)$	4.1	4.5	4.1	4.1	4.3
$(H_3C)_2C{=}O + HOO^\bullet$	14.0	14.0	13.8	14.1	14.1

[a] The conformers are named as in Table 1. All reactant conformers have mirror images of equal energy and are included in the TST calculations. [b] The E_{rel} values of the $CH_3CH(OH)OO^\bullet$ conformers with respect to the lowest-lying are computed at the B3LYP/cc-pVTZ level. [c] The approximate G2M*c*//DFT results were obtained by extrapolation, using the average differences between G2M*a*//DFT, G2M*b*//DFT, and G2M*c*//DFT as found for the methyl- and ethyl-derived radicals in Tables 1 and 3; The hindered internal rotations in acetone were treated appropriately in the TST calculations; the corresponding ZPE modification increases the endothermicity by 0.1 kcal/mol.

TABLE 5: Relative Energies (kcal/mol), ZPE-Corrected, of Stationary Points on the PES of the α-Hydroxy-*cyclo*-hexylperoxyl Reaction *cyclo*-$C_6H_{10}(OH)OO^\bullet \rightleftharpoons$ *cyclo*-$C_6H_{10}O + HO_2^\bullet$ at the G2M*a*//DFT and Approximated G2M*c*//DFT Levels of Theory

structure[a]	G2M*a*//DFT[b,c]	upgraded to approximate G2M*c*/DFT[b,c]
$Q^\bullet OH$_eq + O_2	40.4	40.0
$Q^\bullet OH$_ax + O_2	41.7	41.2
$Q(OH)OO^\bullet$_OHax_mp	0.0	0.0
$Q(OH)OO^\bullet$_OHeq_mp	0.2	0.2
$Q(OH)OO^\bullet$_OHax_tp	1.7	1.7
$Q(OH)OO^\bullet$_OHeq_mm	2.2	2.2
$Q(OH)OO^\bullet$_OHax_mm	2.5	2.5
$Q(OH)OO^\bullet$_OHeq_tp	4.6	4.6
TS*a*_eq	12.9	11.45
TS*a*_ax	13.6	12.15
c-$(Q{=}O^\bullet\cdot\cdot HOO^\bullet)$	5.7	5.85
$Q{=}O + HOO^\bullet$	15.8	16.0

[a] The conformers are named as in Table 1; _ax and _eq denote the axial or equatorial position. All reactant conformers have mirror images of equal energy and are included in the TST calculation [b] The E_{rel} values of the $Q(OH)OO^\bullet$ conformers are calculated at the B3LYP/cc-pVTZ level. [c] G2M*a*//DFT was upgraded to the G2M*c*//DFT level using the systematic difference between G2M*a* and G2M*c* found for the methyl- and ethyl-derived radicals.

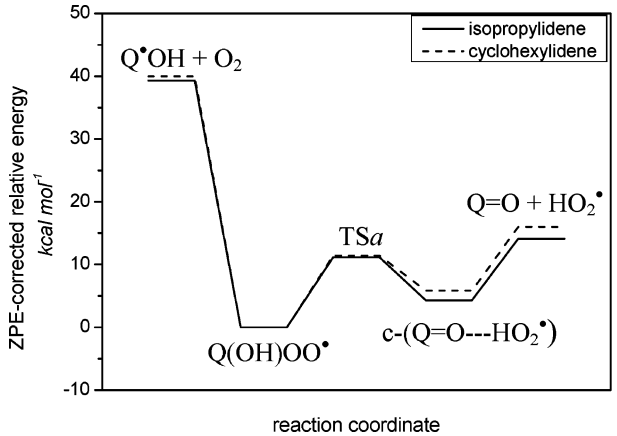

Figure 2. PES of the $Q(OH)OO^\bullet \rightleftharpoons Q{=}O + HO_2^\bullet$ reaction at the approximated G2M*c*//DFT level (see text) for Q = $(CH_3)_2C$ and *cyclo*-C_6H_{10} (*cyclo*-hexylidene), in kilocalories per mole. Only the lowest conformers of $Q(OH)OO^\bullet$ and of TS*a* are shown.

TABLE 6: MC-TST-Calculated Rate Constants, k_{+1} and k_{-1}, for Q(OH)OO• ⇌ Q=O + HO_2• Reactions at Different Temperatures, *T*

Q group	CH_2		CH_3CH		$(CH_3)_2C$		*cyclo*-C_6H_{10}	
T	k_{+1} (s^{-1})	k_{-1} (cm^3 s^{-1})	k_{+1} (s^{-1})	k_{-1} (cm^3 s^{-1})	k_{+1} (s^{-1})	k_{-1} (cm^3 s^{-1})	k_{+1} (s^{-1})	k_{-1} (cm^3 s^{-1})
200	2.3×10^{-3}	3.0×10^{-12}	7.0×10^{-2}	1.5×10^{-12}	1.8×10^{0}	6.9×10^{-12}	5.0×10^{-1}	3.4×10^{-11}
300	2.0×10^{2}	3.2×10^{-13}	2.7×10^{3}	1.9×10^{-13}	2.9×10^{4}	4.8×10^{-13}	1.1×10^{4}	7.9×10^{-13}
400	5.7×10^{4}	1.1×10^{-13}	5.1×10^{5}	7.8×10^{-14}	3.6×10^{6}	1.5×10^{-13}	1.7×10^{6}	1.4×10^{-13}
500	1.6×10^{6}	6.7×10^{-14}	1.2×10^{7}	5.0×10^{-14}	6.3×10^{7}	8.7×10^{-14}	3.4×10^{7}	5.6×10^{-14}
600	1.5×10^{7}	5.1×10^{-14}	9.3×10^{7}	4.0×10^{-14}	4.2×10^{8}	6.7×10^{-14}	2.5×10^{8}	3.4×10^{-14}

TABLE 7: Rate Constant, k_{+1}, and Equilibrium Constant, K_1, for the Various Q(OH)OO• ⇌ Q=O + HO_2• Reactions, Expressed as *A* exp(−*E*/*RT*) for *T* = 200−600 K, and K_{-1} at 210 K

Q group	k_{+1} (s^{-1})	K_1 (cm^{-3})	K_{-1}(210 K) (cm^3)
CH_2	1.28×10^{12} exp(−13.5 kcal mol^{-1}/RT)	2.25×10^{26} exp(−15.9 kcal mol^{-1}/RT)	1.6×10^{-10}
CH_3CH	3.46×10^{12} exp(−12.5 kcal mol^{-1}/RT)	6.34×10^{26} exp(−14.7 kcal mol^{-1}/RT)	3.1×10^{-12}
$(CH_3)_2C$	6.38×10^{12} exp(−11.4 kcal mol^{-1}/RT)	1.28×10^{27} exp(−14.3 kcal mol^{-1}/RT)	6.0×10^{-13}
cyclo-C_6H_{10}	5.55×10^{12} exp(−11.9 kcal mol^{-1}/RT)	6.55×10^{27} exp(−16.1 kcal mol^{-1}/RT)	8.7×10^{-12}

QB3 levels, except for the smallest CH_2(OH)OO• reactant where G3 gives a slightly different result, perhaps due to the low-level HF/6-31G* zero-point-energy (ZPE) correction used in this method.[17]

2. Thermal Rate Constants from Transition State Theory (TST). The overall thermal decomposition rate constant of the Q(OH)OO• → Q=O + HO_2• reaction is given by $k_{+1} = k_{+a}k_{+b}/(k_{-a} + k_{+b})$, where $k_{+b}/(k_{-a} + k_{+b})$ is the fraction of hydrogen-bonded complexes formed in step *a* that dissociates to the final products. k_{+a} was calculated using MC-TST, based on the B3LYP/cc-pVTZ geometries and energy spacings between the different reactant rotamers; all thermally populated reactant conformers and/or transition structures were included, and the critical energies were evaluated at the (approximated) G2M*c*// DFT level (see the Computational Section). The rate constant k_{+b} was calculated according to variational transition state theory (VTST).[22] First, we localized the bottleneck TS (see the Computational Section) at the B3LYP/6-311++G(d,p) level; next, with the critical reaction coordinate thus fixed, the structure was reoptimized at the B3LYP/cc-pVTZ level. It turned out that k_{+b} is always much larger than k_{-a}, even at room temperature; for example, for CH_2(OH)OO• ⇌ CH_2=O + HO_2•, k_{-a}(298 K) = 2.89×10^7 s^{-1} and k_{+b}(298 K) = 7.23×10^9 s^{-1}. Thus, it is reasonable to assume that the overall decomposition rate constant, k_{+1}, equals k_{+a}.[8] It is the very loose structure of TS*b* (O• • •HO_2• distance ≈3.4 Å for the *T* range 300−600 K) which accounts for the extremely fast decomposition of the cyclic intermediate *c*-(Q=O• • •HOO•) complex to Q=O + HO_2•. As all investigated Q(OH)OO• radicals are characterized by an analogous PES (see section 1), it can be concluded that $k_{+1} = k_{+a}$ for all Q(OH)OO• species. The TST-calculated rate coefficients, k_{+1} and k_{-1}, listed in Table 6, demonstrate that both reactions are very fast, outrunning any other possibly competing reactions, such as hydrogen abstractions in liquid-phase autoxidation.[11] Table 6 also invalidates the literature view that the reaction of HO_2• with ketones would be negligibly slow (k_{-1}(298 K) ≤ 8×10^{-16} cm^3 s^{-1}),[9] surmised to be due to the absence of a formyl hydrogen atom.[9] Acetone, for example, reacts at least as fast with HO_2• (k_{-1}(300 K) = 4.8×10^{-13} cm^3 s^{-1}) as aldehydes do, which is consistent with the lack of any critical role for the formyl hydrogen of aldehydes in the addition (see also Figure 1). The reason the very fast reaction of HO_2• with ketones entirely escaped observation thus far in flow tube experiments is the very fast decomposition of the RR′C(OH)-OO• radicals, for example, k_{+1}(300 K) = 2.9×10^4 s^{-1} for $(CH_3)_2$C(OH)OO•, that is, 1−2 orders of magnitude faster than for CH_2(OH)OO• [4] and CH_3CH(OH)OO• [5] radicals.

As a result of the large forward and reverse rate constants, k_{+1} and k_{-1}, Q(OH)OO• radicals can rapidly attain an equilibrium with the corresponding carbonyl compound Q=O and HO_2•. The equilibrium constant K_1 = {[Q=O][HOO•]}/[Q(OH)-OO•] was evaluated as the ratio of partition functions and equals the ratio k_{+1}/k_{-1}. The TST-calculated rate coefficient, k_{+1}, as well as K_1 can be expressed by the Arrhenius-type equations (200−600 K) given in Table 7.

3. Comparison between Theory and Experiment. *(a) CH_2(OH)OO• ⇌ CH_2O + HO_2•.* Before we can compare our TST-calculated rate constant, k_{+1}, with the measured rate constant (*T* = 308 K; pressure 127 Torr air),[4] the falloff factor k(127 Torr)/k_∞ needs to be evaluated. Adopting a collision efficiency factor of $\beta_c = 0.25$, corresponding[24] to an average energy transfer per collision, $\langle\Delta E\rangle$, of −120 cm^{-1} in air (at 308 K),[25] this falloff factor was found to be 0.60, reducing our TST-calculated $k_{+1,\infty}$(308 K) = 362 s^{-1} to k_{+1}(308 K, 127 Torr air) = 217 s^{-1}. This value, derived entirely from first principles, is in perfect agreement with the experimental value 200 ± 100 s^{-1}. An uncertainty on the theoretical rate coefficient of a factor of 5 at room temperature is however to be expected, as the current highest levels of theory can predict barriers only within ∼1 kcal/mol accuracy. Also, our calculated equilibrium constant, K_1(308 K) = 1.5×10^{15} cm^{-3}, is in accord with the experimental {[H_2C=O][HO_2•]}/[CH_2(OH)OO•] value (3.2 ± 1.7) × 10^{15} cm^{-3} at 308 K.[4]

(b) CH_3CH(OH)OO• ⇌ CH_3CHO + HO_2•. Tomas et al.[5] studied this reaction at 298 K and a total pressure of 1 atm of O_2/N_2, measuring k_{+1} = 1870 ± 300 s^{-1}. Using a RRKM-calculated falloff factor of 0.94, our predicted rate constant value k_{+1}(298 K, 1 atm) = 2130 s^{-1} is in excellent agreement with the experimental result. Likewise, our calculated equilibrium constant, K_1(298 K), of 1.05×10^{16} cm^{-3} is again in accord with the experimental value (1.7 ± 1.3) × 10^{16} cm^{-3}.[5]

(c) Preliminary Conclusions. The very good mutual agreement of the three state-of-the-art quantum-chemical methods presented in section 1 and the excellent agreement of the resulting TST rate constants with the available experimental data (section 3) justify our G2M//DFT approach and validate the entire computational procedure used here as an accurate predictive tool for the kinetics of the α-hydroxy-alkylperoxyl radical reactions at issue.

Atmospheric Implications

1. α-Hydroxy-alkylperoxyl Radicals from Alcohols under Atmospheric Conditions. Q(OH)OO• radicals are formed in the atmospheric oxidation of alcohols under normal conditions

as well as in the moderate-temperature consecutive (aut)-oxidation of hydrocarbons. After hydroxyl or peroxyl radicals ($HO_x^\bullet$ or $RO_x^\bullet$) abstract the α-hydrogen atom from an alcohol, oxygen will add rapidly to the resulting α-hydroxyalkyl radical:

$$R{-}OH + {}^\bullet OH \text{ (or } RO_2^\bullet) \rightarrow Q^\bullet OH + H_2O \text{ (or } RO_2H) \quad \text{(r.2)}$$

$$Q^\bullet OH + O_2 \rightarrow Q(OH)OO^\bullet \quad \text{(r.3)}$$

The addition of O_2 to the carbon-centered radical releases about 35−40 kcal/mol, thus producing chemically activated Q(OH)-$OO^{\bullet\dagger}$ radicals. These can either *promptly* decompose to Q═O + $HO_2^\bullet$ (r.1), or *promptly* redissociate to $Q^\bullet(OH) + O_2$ (r.−3), or undergo collisional stabilization by energy transfer to the bath gas. The overall product distributions of the chemically activated reaction systems at hand were derived by performing weak-collision master equation analyses, using an exact stochastic method (ESM) that was validated against the rigorous DCPD and CSSPI methods.[23] The energy distribution of formation, $F_f(E)$, of $Q(OH)OO^\bullet$ from $Q^\bullet OH + O_2$ was derived from detailed balance considerations.[20] The microcanonical rate coefficients, $k_1(E)$ ($\approx k_a(E)$) and $k_{-3}(E)$, of the two unimolecular reactions involved were obtained using RRKM theory.[20] The chemically activated $Q(OH)OO^{\bullet\dagger}$ radicals contain such high internal energies (over 35−40 kcal/mol) that their various rotameric conformers may readily interconvert, as the barriers to the internal rotations around the OO−QO and HO−QO axes amount to only 1−4 kcal/mol. For this reason, in the RRKM expressions for $k_1(E)$ and $k_{-3}(E)$, the densities of internal states, $N(E)$, of $Q(OH)OO^{\bullet\dagger}$ were approximated as the geometric average of the densities calculated assuming the relevant modes to be (i) free internal rotations and (ii) normal vibrations (in this last case, summing over all rotamers). This procedure makes perfect sense here, as the ratio of these two $N(E^\dagger)$ turns out to be about 0.6. The $k_{-3}(E)$ values for prompt redissociation of $HOCH_2OO^{\bullet\dagger}$ were obtained by a microvariational treatment,[22] that is, by locating the bottleneck "TS" structure that minimizes the sum of accessible internal states at the (average) nascent energy, $E^\dagger$; even for this smallest radical, we found $k_{-3}(E) \ll k_1(E)$. For the larger $Q(OH)OO^{\bullet\dagger}$ radicals, for which prompt redissociation is even less competitive, a same bottleneck O−C−O−O geometry was assumed as for the HO−CH_2−O−O$^\bullet$ TS. It may be noted that for the prompt-decomposition reaction (r.1)—which predominates in all cases—overall molecular rotation effects are negligible, as the ratio of the products of the moments of inertia for TS*a* over reactant $Q(OH)OO^\bullet$ is almost unity. For the collisional energy-transfer probabilities, $P(E,E')$, we adopted the standard biexponential Troe model,[24] with the *average* energy transfer per collision in air, $\langle\Delta E\rangle$, taken to be −130 or −250 cm^{-1} as lower and upper limits.[25] The Lennard-Jones collision numbers in air were chosen as follows: Q = CH_2, $Z_{LJ} = 3.0 \times 10^{-10}$ cm^3 s^{-1}; Q = CH_3CH, $Z_{LJ} = 3.5 \times 10^{-10}$ cm^3 s^{-1}; Q = $(CH_3)_2C$, $Z_{LJ} = 4.0 \times 10^{-10}$ cm^3 $molecule^{-1}$ s^{-1}; Q = *cyclo*-C_6H_{10}, $Z_{LJ} = 4.5 \times 10^{-10}$ cm^3 $molecule^{-1}$ s^{-1}.

The product distributions thus obtained by ESM master equation analysis are summarized in Tables 8−11. The number of trials was chosen at 10^7 in order to get reasonable statistics also for minor channels. It can be seen that for the chemically activated C_1-, C_2-, and C_3-α-hydroxy-alkylperoxyl† radicals, collisional stabilization is entirely negligible, whereas the Q═O + $HO_2^\bullet$ prompt-decomposition products constitute more than 99% of the reaction flux. In the case of Q = *cyclo*-hexylidene (Table 11), some stabilization was found, due to the longer $Q(OH)OO^{\bullet\dagger}$ lifetime partly as a result of ring strain in TS*a* leading to the cyclic ketone. The lifetime of the activated $CH_2(OH)OO^{\bullet\dagger}$, $CH_3CH(OH)OO^{\bullet\dagger}$, $(CH_3)_2C(OH)OO^{\bullet\dagger}$, and *c*-$C_6H_{10}(OH)OO^{\bullet\dagger}$ radicals was found to be ∼45, 63, 46, and 285 ps, respectively, the first in agreement with Dibble's value.[8] At lower temperatures and pressures (≈230 K and ≈0.25 atm) as in the upper troposphere, even less stabilization is occurring. Note that the calculated product distribution remains unaffected when steps −*a* and +*b* are included in the analysis, in agreement with our finding for the thermal reactions that $k_{+b} \gg k_{-a}$ such that the overall decomposition rate constant, k_{+1}, is governed entirely by the first step +*a*.

TABLE 8: Calculated Product Distribution, in %, for the $^\bullet CH_2OH + O_2 \rightarrow CH_2(OH)OO^\bullet$ System at 298 K and 1 atm of Air

$\langle\Delta E\rangle$ (cm^{-1})	$^\bullet CH_2OH + O_2$	$CH_2(OH)OO^\bullet$	$H_2C{=}O + HOO^\bullet$
−130[a]	0.7049	<0.0001	99.2951
−250[a]	0.6877	0.0018	99.3105
−250[b]	0.6877	0.0018	99.3105

[a] An artificial sink that "collects" stabilized $Q(OH)OO^\bullet$ radicals is located at the level of TS_a. [b] The sink is located at 7 kcal/mol below TS*a*.

TABLE 9: Calculated Product Distribution, in %, for the $CH_3{}^\bullet CHOH + O_2 \rightarrow CH_3CH(OH)OO^\bullet$ System at 298 K and 1 atm of Air[a]

$\langle\Delta E\rangle$ (cm^{-1})	$CH_3CH^\bullet OH + O_2$	$CH_3CH^\bullet(OH)OO$	$CH_3CH{=}O + HOO^\bullet$
−130	0.0016	0.0002	99.9982
−250	0.0014	0.0270	99.9716

[a] The sink is located at TS*a*.

TABLE 10: Calculated Product Distribution, in %, for the $(CH_3)_2C^\bullet OH + O_2 \rightarrow (CH_3)_2C(OH)OO^\bullet$ System at 298 K and 1 atm of Air[a]

$\langle\Delta E\rangle$ (cm^{-1})	$(CH_3)_2C^\bullet OH + O_2$	$(CH_3)_2C(OH)OO^\bullet$	$(CH_3)_2C{=}O + HOO^\bullet$
−130	0.0017	0.0001	99.9982
−250	0.0017	0.0120	99.9863

[a] The sink is located at TS*a*.

TABLE 11: Calculated Product Distribution, in %, for the *cyclo*-$C_6H_{10}OH + O_2 \rightarrow$ *cyclo*-$C_6H_{10}(OH)OO^\bullet$ System at 298 K and 1 atm of Air[a]

$\langle\Delta E\rangle$ (cm^{-1})	$c\text{-}C_6H_{10}{}^\bullet OH + O_2$	$c\text{-}C_6H_{10}(OH)OO^\bullet$	$C_5H_{10}C{=}O + HOO^\bullet$
−130	<0.001	1.6158	98.3842
−250	<0.001	7.6612	92.3388

[a] The sink is located at TS*a*.

In separate work on the hot, six-ring-opened, C_{10} α-hydroxy-alkylperoxyl† radicals resulting from the $^\bullet$OH-initiated oxidation of α-pinene,[26] we derived approximate stabilization yields under ambient atmospheric conditions as high as 75−90%;[27] these sizeably higher stabilization fractions are in keeping with the longer, ≈1 ns, prompt-decomposition lifetimes (reaction r.1†) and the higher Z_{LJ} collision numbers of these larger $C_{10}{}^\dagger$ structures.

Note that the collisionally stabilized $Q(OH)OO^\bullet$ radicals may still undergo *thermal* decomposition (reaction r.1) but that this process occurs on a time scale of 0.05−5 ms at 300 K (see Table 6), that is, at least 5 orders of magnitude longer than their lifetime for *prompt* decomposition.

2. $HO_2^\bullet$-Initiated Oxidation of Carbonyl Compounds in the Upper Troposphere−Lower Stratosphere (UTLS).

(a) Mechanisms and Effective Removal Rates. We now address thermal Q(OH)OO• radicals formed by the addition of HO_2• to carbonyls Q═O (reaction r.−1). Provided that the thermal decomposition (reaction r.1) is much faster than all other reactions of Q(OH)OO•, reactions r.−1 and r.1 should result in a fast (pre-)equilibrium. The data in Tables 6 and 7 indicate that throughout the earth's planetary boundary layer and free troposphere, down to temperatures of $T \geq 240$ K, the equilibrium concentration of Q(OH)OO• radicals from HO_2• addition to C_1-C_3 carbonyl compounds remains negligibly small, given the prevailing [HO_2•] of the order of 10^7 cm^{-3}. Yet, the equilibrium [Q(OH)OO•] increases exponentially with $1/T$ and should become chemically significant for temperatures ≤220 K. In a recent communication,[13] we reported on the important consequences of this equilibrium shift for the case of $(CH_3)_2C$═O + HO_2• ⇌ $(CH_3)_2C(OH)OO$•. At temperatures ≤220 K, as near the earth's tropopause, the $(CH_3)_2C(OH)OO$• equilibrium concentration was predicted to be sufficiently high for the subsequent reactions with NO and, to a lesser extent, with HO_2• to result in important acetone removal, on a par with the direct $(CH_3)_2C$═O reaction with •OH, and even competing with acetone photolysis. The oxy radical from the reaction with NO can only undergo very fast β C—C cleavage (barrier <8 kcal/mol[28]) to produce acetic acid:

$$(CH_3)_2C(OH)OO^\bullet + NO \rightarrow (CH_3)_2C(OH)O^\bullet + NO_2 \quad \text{(r.4)}$$

$$(CH_3)_2C(OH)O^\bullet \rightarrow CH_3COOH + {}^\bullet CH_3 \quad \text{(r.5)}$$

The reaction with HO_2• is less important but constitutes in part a radical termination route (r.6a) that affects the local HO_x budget:

$$(CH_3)_2C(OH)OO^\bullet + HO_2^\bullet \rightarrow (CH_3)_2C(OH)OOH + O_2 \quad \text{(r.6a)}$$

$$\rightarrow \text{other products} \quad \text{(r.6b)}$$

At (r.−1), (r.1) equilibrium, the net acetone loss rate can be expressed as

$$k_{eff} = K_{-1}[HO_2^\bullet]\{k_4[NO] + k_6[HO_2^\bullet]\} \quad (1)$$

characterized by a sharp negative temperature dependency through K_{-1}. The rate constant k_4(≈200 K) for RO_2• + NO reactions is known to be ≈1.5×10^{-11} cm^3 s^{-1}, while k_6(≈200 K) can be estimated at ≈1×10^{-10} cm^3 s^{-1} from the known data for $HOCH_2OO$• + HO_2•.[29] As an example, we consider the wintertime tropopause (altitude ≈10 km) for temperate Northern latitudes (40−50° N) above polluted continental areas (NO levels 40−80 ppt), with approximate diurnal averages: [NO] ≈ 5×10^8, [HO_2•] ≈ 1×10^7, and [•OH] ≈ 2.5×10^5 cm^{-3} (see, e.g., ref 30). Below, we adopt $T = 210$ K. Using our predicted K_{-1}(210 K) = 6×10^{-13} cm^3 (see Table 7), we find an HO_2•-initiated acetone removal rate of $k_{eff} = 5 \times 10^{-8}$ s^{-1}. This is of the same order as the rates of the known acetone sinks: (i) 3.8×10^{-8} s^{-1} for the reaction with •OH, with a rate coefficient at 210 K of 1.5×10^{-13} cm^3 s^{-1},[31] and (ii) ≤5×10^{-8} s^{-1} for photolysis (diurnal average), using the recently revised data.[32] It must be stressed that temperature is a crucial factor for this new removal mechanism: a T difference of 10° changes the rate k_{eff} by a factor of 7, implying that, under the conditions above, this mechanism would become dominant at 200 K but, conversely, only minor at 220 K. As just 20° makes a factor of 50 in the balance, it is clear that the diurnal T variations and meteorological fluctuations should be taken into account. It may be noted that measurements of Arnold and coworkers in the UTLS at 50° N, above Germany, not only reveal a close correlation between acetic acid and acetone but also show the acetic acid mixing ratio to maximize around a 9 km altitude,[33] that is, close to the altitude where the efficiency of our HO_2•-initiated acetone oxidation path is expected to be highest.

As for larger ketones, an interesting case is *cyclo*-hexanone, which can also serve as a template for nopinone, a major oxidation product of β-pinene.[34] The HO_2• addition to this cyclic ketone is somewhat more exoergic (16.0 kcal/mol, see Table 5) due to the ring-strain relaxation, such that the predicted K_{-1}(210 K) is large: 9×10^{-12} cm^3 (Table 7). Under the same conditions as above, this leads to a k_{eff} value for the HO_2•-initiated removal of 7.5×10^{-7} s^{-1}. This is almost equal to the loss rate 9×10^{-7} s^{-1} by reaction with •OH, using a rate coefficient of k(210 K) ≈ 3.5×10^{-12} cm^3 s^{-1} as follows from current structure−activity relations.[35]

As far as acetaldehyde is concerned, K_{-1}(210 K) for the HO_2• addition is only about 5 times larger than that for acetone (Table 7), whereas the rate coefficient of the •OH reaction is 150−200 times larger.[29,36] As a result, again under the same conditions as above, the •OH reaction should outrun the reaction with HO_2• at 210 K by a factor of 20−30.

However, matters are quite different for formaldehyde, the smallest and by far most important aldehyde in atmospheric chemistry (global source strength ≈1500 Tg/year estimated from source strengths of major precursors using the IMAGES model; see below). First, the $CH_2(OH)OO$• adduct is found to be both unusually stable and entropically favored (see Tables 1 and 2 and 6 and 7), such that K_{-1} is exceptionally large: K_{-1}(210 K) = 1.6×10^{-10} cm^3, that is, 270 times that for acetone and 50 times that for acetaldehyde. This off-sets both the high rate coefficient of the •OH reaction, ≈1.0×10^{-11} cm^3 s^{-1} at 210 K,[36] and, to some extent, also the exceptionally high photolysis rate (wintertime diurnal average at 40−50° N) ≈3.5×10^{-5} s^{-1}.[37] On the other hand, at $T \leq 210$ K, the rather slow $CH_2(OH)OO$• → HO_2• + CH_2O redissociation is no longer fast enough to still dominate the fate of the adduct and to maintain the equilibrium: k_1(210 K) = 1.1×10^{-2} s^{-1} (see Table 7), whereas the rate of irreversible $CH_2(OH)OO$• removal is {k_4[NO] + k_6[HO_2•]} = 9×10^{-3} s^{-1} for the conditions and rate coefficients considered above. Therefore, the net HO_2•-initiated removal rate is given here by the following steady state expression:

$$k_{eff} = k_{-1}[HO_2^\bullet]\{k_4[NO] + k_6[HO_2^\bullet]\}/\{k_1 + k_4[NO] + k_6[HO_2^\bullet]\} \quad (2)$$

Thus, always for the wintertime, temperate-latitude, polluted conditions as above, and with k_{-1} and k_1 at 210 K from Tables 6 and 7, we find for the HO_2•-initiated oxidation of CH_2O k_{eff} = 1.1×10^{-5} s^{-1}, that is, much larger than the 2.5×10^{-6} s^{-1} loss rate by •OH at [•OH] = 2.5×10^5 cm^{-3} and approaching the diurnally averaged wintertime photolysis rate of ≈3.5×10^{-5} s^{-1}. Note that the $CH_2(OH)O$• oxy radical formed in the NO reaction is expected to react mainly if not exclusively with O_2, yielding HO_2• and formic acid, HCOOH.

(b) IMAGES Model Calculations. The impact of the reaction of HO_2• with acetone and formaldehyde on the composition of the troposphere has been estimated using the IMAGES model.[38,39] This model calculates the global distributions of 60 tropospheric compounds, including the main compounds influencing the

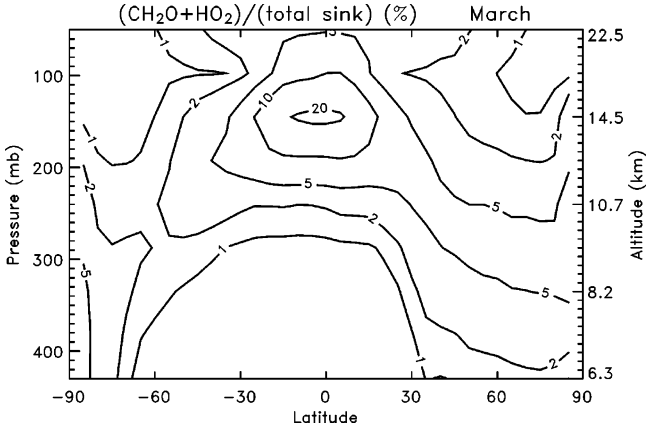

Figure 3. Zonally averaged relative contribution (in percent) of the $HO_2^\bullet + CH_2O$ reaction to the total sink of formaldehyde in the UTLS, estimated using the IMAGES model for the month of March.

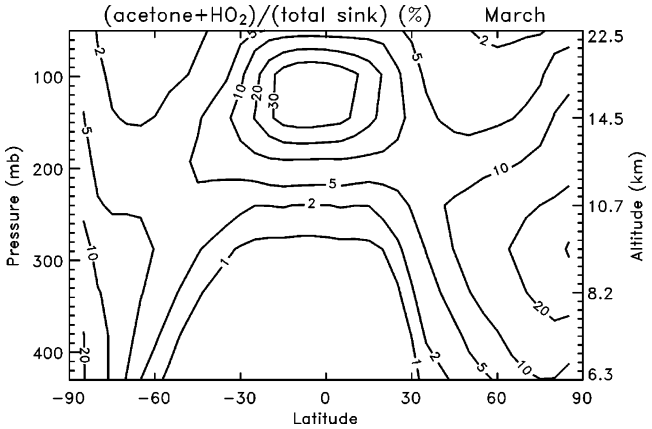

Figure 4. Zonally averaged relative contribution (in percent) of the $HO_2^\bullet + CH_3COCH_3$ reaction to the total sink of acetone in the UTLS, estimated using the IMAGES model for the month of March.

budget of ozone and the hydroxyl radical in the troposphere. Its resolution is 5° × 5° in the horizontal, with 25 levels extending between the earth's surface and the 50 hPa level. The meteorological fields used to drive the model transport and the calculation of kinetic rates are monthly averages derived from a 5 year climatology from the European Centre for Medium-Range Weather Forecasts (ECMWF), as described in ref 38.

The reactions of the radicals $CH_2(OH)OO^\bullet$ and $(CH_3)_2C(OH)OO^\bullet$ produced through the reactions of formaldehyde and acetone with $HO_2^\bullet$ have been included in the model, using the decomposition rates and equilibrium constants determined in this study (Table 7) and the rate constants of the subsequent reactions with NO and $HO_2^\bullet$ mentioned in the previous section.

Note that further reactions of the hydroperoxides formed from the latter reactions are neglected in the model, although they are expected to produce in part the initial α-hydroxy-alkylperoxy radical, a fraction of which decomposes to either acetone or formaldehyde + $HO_2^\bullet$, thereby reducing the overall loss rate of the carbonyl through the whole reaction cycle.

The relative contribution of the $HO_2^\bullet$ reactions to the total sink of formaldehyde and acetone is represented in Figures 3 and 4, as a function of latitude and pressure for the month of March. It is found to be significant at and just below the tropical tropopause, in the 100−150 hPa pressure range, where the temperatures are lowest (around 200 K when diurnally averaged) and $HO_2^\bullet$ levels are in the range $(0.5-4) \times 10^7$ molecules cm^{-3} during the daytime. At higher latitudes, the average contribution of the $HO_2^\bullet$ reaction is smaller (despite the lower photolysis rates and $^\bullet OH$ levels at these latitudes), primarily because of the warmer average temperatures (>220 K) prevailing around the tropopause in these regions in March.

The carbonyl + $HO_2^\bullet$ reactions lead to significant decreases in the carbonyl and $HO_x^\bullet$ abundances around the tropopause: up to 30% at 145 hPa for both CH_2O and acetone and even more at and above the tropopause in the case of acetone. The abundances of $^\bullet OH$ and $HO_2^\bullet$ are depressed by as much as 6 and 12% around the equator in the 100−150 hPa pressure range, respectively. The global sinks of the carbonyls due to reaction with $HO_2^\bullet$ are estimated to be 10 Tg(CH_2O)/year and 1.1 Tg(acetone)/year. Hydroperoxide production, through the reaction $Q(OH)OO^\bullet + HO_2^\bullet \rightarrow Q(OH)OOH + O_2$, represents only 25−30% of this sink, so that the role of the subsequent reactions of these species is expected to be small. The remainder is provided by formic and acetic acid production.

Note, however, that the role of temperature variations over the course of the day is neglected in these calculations. This impact can be roughly estimated using the radar measurements of temperature at the Indian station Gadanki (13.5° N, 79.2° E).[40] Figure 5a shows the observed diurnal evolution of temperature about 2 km below the local tropopause (15 km altitude), that is, where organic acid production is predicted to be maximum. The loss rates of formaldehyde and acetone shown in Figure 5b and c have been calculated using these measured temperatures and the modeled concentrations of $OH^\bullet$, $HO_2^\bullet$, and NO at the closest model grid point. Using these results, it is estimated that the use of diurnally averaged temperatures in the IMAGES model leads to an overestimation of the net formaldehyde and acetone sinks, by factors of 1.4 and 1.6, respectively.

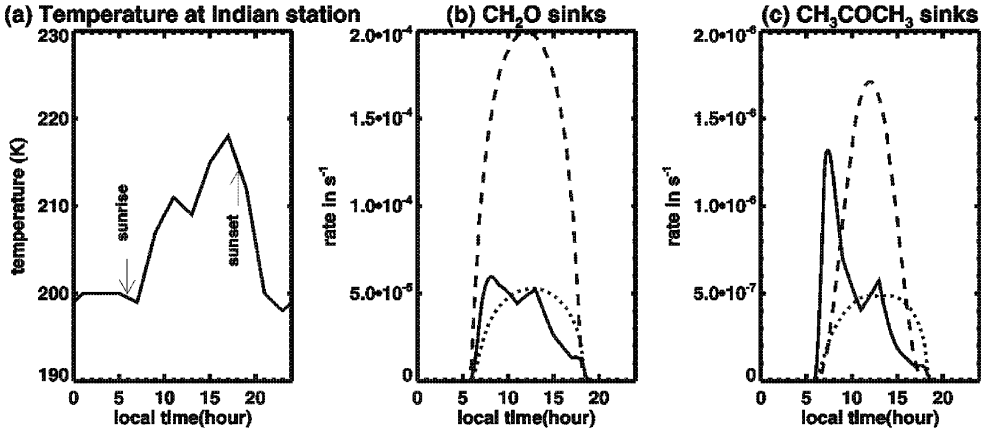

Figure 5. (a) Measured temperatures at a 15 km altitude on August 24−25 at Gadanki, India,[40] (b) calculated loss rates of CH_2O (in inverted seconds) due to the $HO_2^\bullet$ reaction (solid line), the $^\bullet OH$ reaction (dotted line) and photolysis (dashed line), and (c) same for CH_3COCH_3.

It follows that our best estimates for the global sink due to reaction with $HO_2^\bullet$ are 7 Tg(CH_2O)/year and 0.7 Tg(acetone)/year. The global production of acids is estimated to be about 8 Tg(HCOOH)/year and 0.5 Tg(CH_3COOH)/year.

Conclusions

Various high quantum-chemical levels—G3, CBS-QB3, and G2M//DFT with CCSD(T)/aug-cc-pVDZ—were found to give nearly identical results for the PES governing the concerted, hydrogen-bond-assisted decomposition of α-hydroxy-alkylperoxyl radicals into $HO_2^\bullet$ and the corresponding aldehyde/ketone: $Q(OH)OO^\bullet \rightleftharpoons HO_2^\bullet + Q{=}O$. State-of-the-art, multiconformer TST calculations on the G2M//DFT PES were found to reproduce the available rate and equilibrium constants for the reactions of both the $CH_2(OH)OO^\bullet$ and $CH_3CH(OH)OO^\bullet$ radicals within the experimental error ($\leq \pm 50\%$), thus attesting to the soundness and reliability of the methodologies brought to bear in this work.

Using these validated theoretical methods, we have shown that the (reverse) reaction of $HO_2^\bullet$ with ketones is as fast as that with aldehydes, whereas the $Q(OH)OO^\bullet$ decomposition is much faster when the product Q=O is a ketone. In all cases, the addition and decomposition reactions are both found to be so fast as to result readily in $HO_2^\bullet + Q{=}O \rightleftharpoons Q(OH)OO^\bullet$ equilibrium.

We have shown that, at the low temperatures near the earth's tropopause, for the carbonyls CH_2O, $(CH_3)_2CO$, and *cyclo*-hexanone, this equilibrium shifts far enough to $Q(OH)OO^\bullet$ that its subsequent reactions with NO and $HO_2^\bullet$ should result in a substantial net carbonyl loss. This hitherto overlooked $HO_2^\bullet$-initated oxidation of carbonyl compounds was further investigated by IMAGES model calculations and shown to be indeed an efficient sink of formaldehyde and acetone as well as a source of formic and acetic acids in the UTLS and to significantly influence the $HO_x^\bullet$ budget near the tropopause. Preliminary results on substituted carbonyl compounds such as hydroxyacetone indicate that their removal via the $HO_2^\bullet$-initiated mechanism may also be of some importance in the UTLS.

It should be emphasized, however, that a possible error of ≈1 kcal/mol on the computed critical energies implies an uncertainty in the predicted rates of a factor of ≈10 at temperatures of 200−220 K. However, this large error estimate appears overly pessimistic, given the excellent agreement of our predicted rate coefficients, k_1 and k_{-1}, at $T \approx 300$ K with the available experimental data[4,5] for CH_2O and CH_3CHO. In any case, it is obvious that the theoretical predictions presented in this work must await experimental verification.

We have also shown that chemically activated $Q(OH)OO^\bullet$ radicals formed by O_2 addition to α-hydroxy-alkyl radicals resulting from the (atmospheric) oxidation of C_1-C_3 alcohols will quasi-exclusively decompose *promptly* into $HO_2^\bullet$ and the corresponding carbonyl, whereas their collisional stabilization is entirely negligible, under all atmospheric conditions.

Acknowledgment. This work was performed in the frame of the FP5 program of the European Commission (UTOPIHAN-ACT project), with additional funding by the Belgian IAP-PAI network, the Belgian OSTC "Global Change" PODO II program, the Flanders BOF-GOA program (through two projects), and an FWO-Flanders project. I.H. and T.L.N. are grateful to the *Fonds voor Wetenschappelijk onderzoek*, Flanders, and to the European Commission (FP5), respectively, for Ph.D. grants. The authors thank Dr L. Vereecken, Department of Chemistry, KULeuven, for useful comments.

Supporting Information Available: Geometries, energies, ZPEs, rotational constants, and vibration frequency data of the discussed structures. This material is available free of charge via the Internet at http://pubs.acs.org.

References and Notes

(1) Atkinson, R. *Atmos. Environ.* **1990**, *24*, 1.

(2) Niki, H.; Maker, P. D.; Savage, C. M.; Breitenbach, L. P. *Chem. Phys. Lett.* **1981**, *80*, 499.

(3) Westbrook, C. L.; Dryer, F. L. *Combust. Sci. Technol.* **1979**, *20*, 215.

(4) Veyret, B.; Lesclaux, R.; Rayez, M. T.; Rayez, J. C.; Cox, R. A.; Moortgat, K. G. *J. Phys. Chem.* **1989**, *93*, 2368.

(5) Tomas, A.; Villenave, E.; Lesclaux, R. *J. Phys. Chem. A* **2001**, *105*, 3505.

(6) Evleth, E. M.; Melius, C. F.; Rayez, M. T.; Rayez, J. C.; Forst, W. *J. Phys. Chem.* **1993**, *97* (19), 5040.

(7) Olivella, S.; Bofill, J. M.; Solé, A. *Chem.—Eur. J.* **2001**, *7*, 3377.

(8) Dibble, T. S. *Chem. Phys. Lett.* **2002**, *355*, 193.

(9) Gierczak, T.; Ravishankara, A. R. *Int. J. Chem. Kinet.* **2000**, *32* (9), 5737.

(10) Tolman, C. A.; Druliner, J. D.; Nappa, M. J.; Herron, N. In *Activation and Functionalization of Alkanes*; Hill, C. L., Ed.; John Wiley & Sons: New York, 1989; p 303.

(11) Hermans, I.; Nguyen, L. T.; Jacobs, P. A.; Peeters, J. *ChemPhysChem* **2005**, DOI: 10.1002/cphc.200400211.

(12) Rowley, D. M.; Lesclaux, R.; Lightfoot, P. D.; Nozière, B.; Wallington, T. J.; Hurley, M. D. *J. Phys. Chem.* **1992**, *96*, 4889.

(13) Hermans, I.; Nguyen, L. T.; Jacobs, P. A.; Peeters, J. *J. Am. Chem. Soc.* **2004**, *126*, 9908.

(14) Frisch, M. J.; Trucks, G. W.; Schlegel, H. B.; Scuseria, G. E.; Robb, M. A.; Cheeseman, J. R.; Montgomery, J. A.; Vreven, T., Jr.; Kudin, K. N.; Burant, J. C.; Millam, J. M.; Iyengar, S. S.; Tomasi, J.; Barone, V.; Mennucci, B.; Cossi, M.; Scalmani, G.; Rega, N.; Petersson, G. A.; Nakatsuji, H.; Hada, M.; Ehara, M.; Toyota, K.; Fukuda, R.; Hasegawa, J.; Ishida, M.; Nakajima, T.; Honda, Y.; Kitao, O.; Nakai, H.; Klene, M.; Li, X.; Knox, J. E.; Hratchian, H. P.; Cross, J. B.; Adamo, C.; Jaramillo, J.; Gomperts, R.; Stratmann, R. E.; Yazyev, O.; Austin, A. J.; Cammi, R.; Pomelli, C.; Ochterski, J. W.; Ayala, P. Y.; Morokuma, K.; Voth, G. A.; Salvador, P.; Dannenberg, J. J.; Zakrzewski, V. G.; Dapprich, S.; Daniels, A. D.; Strain, M. C.; Farkas, O.; Malick, D. K.; Rabuck, A. D.; Raghavachari, K.; Foresman, J. B.; Ortiz, J. V.; Cui, Q.; Baboul, A. G.; Clifford, S.; Cioslowski, J.; Stefanov, B. B.; Liu, G.; Liashenko, A.; Piskorz, P.; Komaromi, I.; Martin, R. L.; Fox, D. J.; Keith, T.; Al-Laham, M. A.; Peng, C. Y.; Nanayakkara, A.; Challacombe, M.; Gill, P. M. W.; Johnson, B.; Chen, W.; Wong, M. W.; Gonzalez, C.; Pople, J. A. *Gaussian 03*, revision B.03; Gaussian, Inc.: Pittsburgh, PA, 2003.

(15) Mebel, A. M.; Morokuma, K.; Lin, M. C. *J. Chem. Phys.* **1995**, *103*, 7414.

(16) Montgomery, J. A., Jr.; Frisch, M. J.; Ochterski, J. W.; Petersson, G. A. *J. Chem. Phys.* **2000**, *112*, 6532.

(17) Curtiss, L. A.; Raghavachari, K.; Redfern, P. C.; Rassolov, V.; Pople, J. A. *J. Chem. Phys.* **1998**, *109*, 7764.

(18) Eyring, H. *J. Chem. Phys.* **1934**, *3*, 107.

(19) (a) Vereecken, L.; Peeters, J. *J. Phys. Chem. A* **1999**, *103*, 1768. (b) Vereecken, L.; Peeters, J. *J. Chem. Phys.* **2003**, *119*, 5159.

(20) Forst W. *Theory of Unimolecular Reactions*; Academic Press: New York and London, 1973.

(21) Chuang, Y.-Y.; Truhlar, D. G. *J. Chem. Phys.* **2000**, *112*, 1221.

(22) See, for example: Holbrook, K.; Pilling, M.; Robertson, S. *Unimolecular Reactions*, 2nd ed.; Wiley: New York, 1996.

(23) Vereecken, L.; Huybrechts, G.; Peeters, J. *J. Chem. Phys.* **1997**, *106*, 6564.

(24) Troe, J. *J. Chem. Phys.* **1977**, *66*, 4745.

(25) Oref, I.; Tardy, D. C. *Chem. Rev.* **1990**, *90*, 1407.

(26) Peeters, J.; Vereecken, L.; Fantechi, G. *Phys. Chem. Chem. Phys.* **2001**, *3*, 5489.

(27) Capouet, M.; Nozière, B.; Peeters, J.; Müller, J.-F. *Atmos. Chem. Phys.* **2004**, *4*, 2285.

(28) Peeters, J.; Fantechi, G.; Vereecken, L. *J. Atmos. Chem.* **2004**, *48*, 59.

(29) Atkinson, R.; Baulch, D. L.; Cox, R. A.; Hampson, R. F.; Kerr, J. A.; Rossi, M. J.; Troe, J. *J. Phys. Chem. Ref. Data* **1997**, *26*, 521.

(30) Hauglustaine, D. A.; Brasseur, G. P.; Walters, S.; Rasch, P. J.; Muller, J. F.; Emmons, L. K.; Carroll, C. A. *J. Geophys. Res. D: Atmos.* **1998**, *103* (21), 28291.

(31) Wollenhaupt, M.; Carl, S. A.; Horowitz, A.; Crowley, J. N. *J. Phys. Chem. A* **2000**, *104*, 2695.

(32) Blitz, M. A.; Heard, D. E.; Pilling, M. J., Arnold, S. R.; Chipperfield, M. P. *Geophys. Res. Lett.* **2004**, *31* (6), L06111.

(33) Reiner, T.; Mohler, O.; Arnold, F. *J. Geophys. Res. D: Atmos.* **1999**, *104* (11), 13943.

(34) Atkinson, R.; Arey, J. *Atmos. Environ.* **2003**, *37* (Suppl. 2), 197.

(35) Kwok, E. S. C.; Atkinson, R. *Atmos. Environ.* **1995**, *29*, 1685.

(36) Atkinson, R.; Baulch, D. L.; Cox, R. A.; Crowley, J. N.; Hampson R. F., Jr.; Kerr, J. A.; Rossi, M. J.; Troe, J. IUPAC Subcommittee on Gas Kinetic Data Evaluation for Atmospheric Chemistry, http://www.iupac-kinetic.ch.cam.ac.uk.

(37) Meller, R.; Moortgat, G. K. *J. Geophys. Res.* **2000**, *105*, 7089.

(38) Müller, J.-F.; Brasseur, G. P. *J. Geophys. Res.* **1995**, *100*, 16445−16490.

(39) Müller, J.-F.; Stavrakou, T. *Atmos. Chem. Phys. Discuss.* **2004**, *4*, 7985.

(40) Revathy, K.; Prabhakaran Nayar, S. R.; Krishna Murthy, B. V. *Ann. Geophys.* **2001**, *19*, 1001.